Cytoskeletal Remodeling during Growth Cone–Target Interactions

Chi-Hung Lin and Paul Forscher

Department of Biology, Yale University, New Haven Connecticut 06511

Abstract. Reorganization of the cytoskeleton of neuronal growth cones in response to environmental cues underlies the process of axonal guidance. Most previous studies addressing cytoskeletal changes during growth cone pathfinding have focused on the dynamics of a single cytoskeletal component. We report here an investigation of homophilic growth cone–target interactions between *Aplysia* bag cell neurons using digitally enhanced video microscopy, which addresses dynamic interactions between actin filaments and microtubules. After physical contact of a growth cone with a physiological target, mechanical coupling occurred after a delay; and then the growth cone exerted forces on and displaced the target object. Subsequent to coupling, F-actin accumulation was observed at the target contact zone, followed by preferential microtubule extension to the same site. After successful target interactions, growth cones typically moved off highly adhesive poly-L-lysine substrates onto native target cell surfaces. These events were associated with modulation of both the direction and rate of neurite outgrowth: growth cone migration was typically reoriented to a trajectory along the target interaction axis and rates of advance increased by about one order of magnitude. Directed microtubule movements toward the contact site appeared to be F-actin dependent as target site-specific microtubule extension and bundling could be reversibly randomized by micromolar levels of cytochalasin B in a characteristic manner. Our results suggest that target contacts can induce focal F-actin assembly and reorganization which, in turn, guides target site–directed microtubule redistribution.

SINCE the early morphological studies of Ramon y Cajal and Harrison (Ramon y Cajal, 1890; Harrison, 1910), the growth cone has been ascribed a major role in axonal guidance and target recognition during development and nerve regeneration. Growth cones are capable of responding to various environmental signals, including electrical fields (Patel and Poo, 1982; Cooper and Schliwa, 1985), soluble trophic or tropic factors (Gundersen and Barrett, 1980; Tessier et al., 1988), molecular cues residing in the extracellular matrix (for review see Reichardt and Tomaselli, 1991), and cell adhesion molecules (for reviews see Dodd and Jessell, 1988; Jessell, 1988; Hortsch and Goodman, 1991; Takeichi, 1991). Axonal guidance and target recognition also involve mechanical interactions between growth cones and specific substrates. Growth cones can exert mechanical force on targets (Bray, 1979; Lamoureux et al., 1989; Heidemann et al., 1990) and conversely, application of external force can influence the rate of neurite elongation (Bray, 1984; Lamoureux et al., 1992). Attempts have been made to elucidate the molecular basis of the forces underlying neurite elongation and steering, and evidence supports roles for both actin filaments and microtubules in a generation of neurite tension and extension (Letourneau et al., 1987; Dennerll et al., 1989). However, a clear picture of the functional role of either of these cytoskeletal elements or their interactions during axonal guidance has yet to emerge.

Complementing work on cytomechanics are studies addressing the role of actin and microtubule dynamics in axonal elongation and guidance. Initial studies in embryonic grasshoppers and cultured neurons demonstrated that actin filament assembly was necessary for accurate pathfinding but not for continued axonal growth (Bentley and Toroian-Raymond, 1986; Letourneau et al., 1987). A recent study suggested a role for microtubules in the guidance process as well (Sabry et al., 1991). These studies raise basic questions regarding both the cytomechanics and cytoskeletal dynamics involved.

Specifically, how do actin filaments interact with microtubules during growth cone–target interactions? How does one cytoskeletal population influence the assembly and localization of the other? These questions are of fundamental importance because microtubules provide not only the structural elements needed for axonal growth but also a means of metabolic support for the nerve terminal and communication with the cell body. Despite abundant evidence suggesting functional interactions between actin filaments and microtubules, most biochemical studies to date have not been conclusive (Griffith and Pollard, 1978; Schliwa and Van Blerkom, 1981; Selden and Pollard, 1983; Travis and Bowser, 1986) and experiments with fluorescent cytoskeletal analogs have generally been restricted to analysis of one filament population at

Please address all correspondence to Dr. P. Forscher, Department of Biology KBT-338, Yale University, P.O. Box 6666, New Haven, CT 06511-8112.

a time (Sabry et al., 1991; Tanaka and Kirschner, 1991; Okabe and Hirokawa, 1991).

We have previously demonstrated that actin filaments influence microtubule distributions in *Aplysia* growth cones in vitro. When growth cones were treated with cytochalasin B to remove actin filaments from the growth cone lamella, microtubules rapidly elongated, moving from the centrally located "transition zone" into the distal lamellar domain (Forscher and Smith, 1988). These studies demonstrated that axonal microtubules have a latent potential for rapid extension and suggested an inhibitory role for actin filaments: the dense peripheral F-actin matrix was either physically excluding microtubules or somehow inhibiting plus end microtubule polymerization. This propensity for microtubule elongation once peripheral F-actin was removed is consistent with independent evidence suggesting that microtubules in the axonal shaft are under compression generated by microfilament-dependent processes (Dennerll et al., 1988, 1989).

One approach which has been particularly useful for the study of cytoskeletal aspects of growth cone guidance is the use of derivatized microspheric beads. Under some circumstances, beads appear to act as pseudotargets, mimicking the actions of physiological substrates. Interactions with polycationic bead surfaces, for example, can trigger morphogenic changes in neurons and muscle cells normally associated with formation of both pre- and postsynaptic specializations (Peng and Cheng, 1982; Peng et al., 1987). Polystyrene microspheres or other particulate membrane markers applied to the surface of growth cones (Bray, 1970; Forscher and Smith, 1990) or other motile cells (Kucik et al., 1989; Sheetz et al., 1989; de Brabander et al., 1991) can also become mechanically coupled to the intracellular retrograde movement of cortical F-actin via interactions with membrane proteins thought to be involved in substrate adhesion and traction. In addition, we have recently shown that highly charged polycationic beads can induce local actin filament assembly at the site of bead binding (Forscher et al., 1992). These studies suggest that pseudotarget interactions can elicit a range of effects on actin-based structures and motility in growth cones that depends on specific experimental conditions.

In this report, we expand our initial studies on growth cone–pseudotarget interactions to include interactions with physiological target substrates. The *Aplysia* bag cell neurons used in this study are neurosecretory cells situated in two clusters in the abdominal ganglion which synthesize peptidergic hormones involved in regulation of egg laying. All the cells in each cluster are normally electrically coupled via gap junctions in situ; this facilitates the synchronous firing of action potentials during a neurosecretory response. Functional gap junctions have been demonstrated between bag cell neurons both in vivo and in vitro (Kaczmarek et al., 1979); thus, the homophilic interactions we report here are likely to be physiologically relevant.

We have documented the cytological remodeling events during homophilic interactions between bag cell neurons and correlated the observed structural changes with underlying cytoskeletal protein redistributions, the locations of which were confirmed at key time points using specific fluorescent probes. The results of these native target interactions were compared and contrasted with responses after pseudotarget (bead) contacts in an attempt to dissect underlying cytomechanical mechanisms. The characteristic temporal sequence of actin reorganization preceding microtubule rearrangement and the sensitivity of directed microtubule movements to cytochalasin treatment all suggest a primary role for actin filaments in mediating microtubule guidance during axonal elongation.

Materials and Methods

Cell Culture

Aplysia californica were provided by Marinus Inc., Long Beach, CA. Dissociated bag cell neurons were plated on poly-L-lysine–coated coverslips in serum-free L-15 medium supplemented with seawater salts (L15–ASW) as previously described (Forscher and Smith, 1988). To promote growth cone–target interactions, bag cell neurons were carefully positioned such that a growth cone could interact with another growth cone or neurites from neighboring cells. Cells were incubated at room temperature for 12–24 h after plating before homophilic interactions among bag cell neurons were examined.

Video-Light Microscopy and Image Processing

A Zeiss Axiovert-10 inverted microscope set up for both differential interference contrast (DIC)[1] and fluorescence observation was used; video images were digitally enhanced by background subtraction and frame averaging as described (Forscher and Smith, 1988). The processed images were recorded on an optical memory laser disk (Panasonic model TQ-2026F), and then redigitized for data analysis and image processing before photographic output onto a 35-mm Kodak Technical Pan Film using a Slide Writer film recorder (AGFA Corp., Orangeburg, NY). The fluorescence images were processed by a 5 × 5 sharpening convolution filter (Adobe Photoshop, Mountain View, CA).

Rate measurements were made using a 151-AT series image processor (Imaging Technology Inc., Woburn, MA) and image analysis programs written in our laboratory. Rates of C-domain or leading edge advance were calculated using 100-s sampling intervals. To precisely localize objects for rate measurement, a centroid program was developed that enabled consistent determination of object positions under DIC microscopy. In practice, this measurement resulted in maximal errors of ~2 pixels, equivalent to 0.27–0.41 μm at the magnifications used in this study. Rates of neurite outgrowth were calculated from observation periods of at least 20 min.

Experimental Treatments

Cells were mounted in custom-made chambers as described (Forscher et al., 1987) and constantly perfused at room temperature with isotonic L15 medium. At key time points during target interactions, the neurons were fixed, and then permeabilized and stained for the presence of F-actin and microtubules as described below. The fixation and permeabilization processes were closely monitored to obtain optimized preservation of fine growth cone structure as described previously (Forscher and Smith, 1988). To address the role of actin dynamics during growth cone–target interactions, cells were treated with 5 μm of cytochalasin B (Sigma Chem. Co., St. Louis, MO), and then extensively washed with L15-ASW. Positively charged polystyrene beads used to measure the rates of retrograde F-actin flow were derivatized with polyethyleneimine as described previously (Forscher and Smith, 1990).

Fluorescent Labeling

The fixation buffer contained isotonic ASW supplemented with 4% freshly made paraformaldehyde and 400 mM sucrose, pH 7.6. After fixation, cells were permeabilized for 2–5 min in fixation buffer plus 0.5% Triton X-100, washed with PBS, and stained with rhodamine-phalloidin (Molecular Probes Inc., Eugene, OR) in PBS. Cells were then washed with PBS, exposed to 5% BSA-PBS followed by monoclonal mouse anti-β-tubulin antibody (Sigma Chem. Co.), washed with PBS, exposed to FITC-conjugated goat anti-rabbit secondary antibody (Jackson ImmunoResearch Labs. Inc.,

1. *Abbreviations used in this paper*: DIC, differential interference contrast.

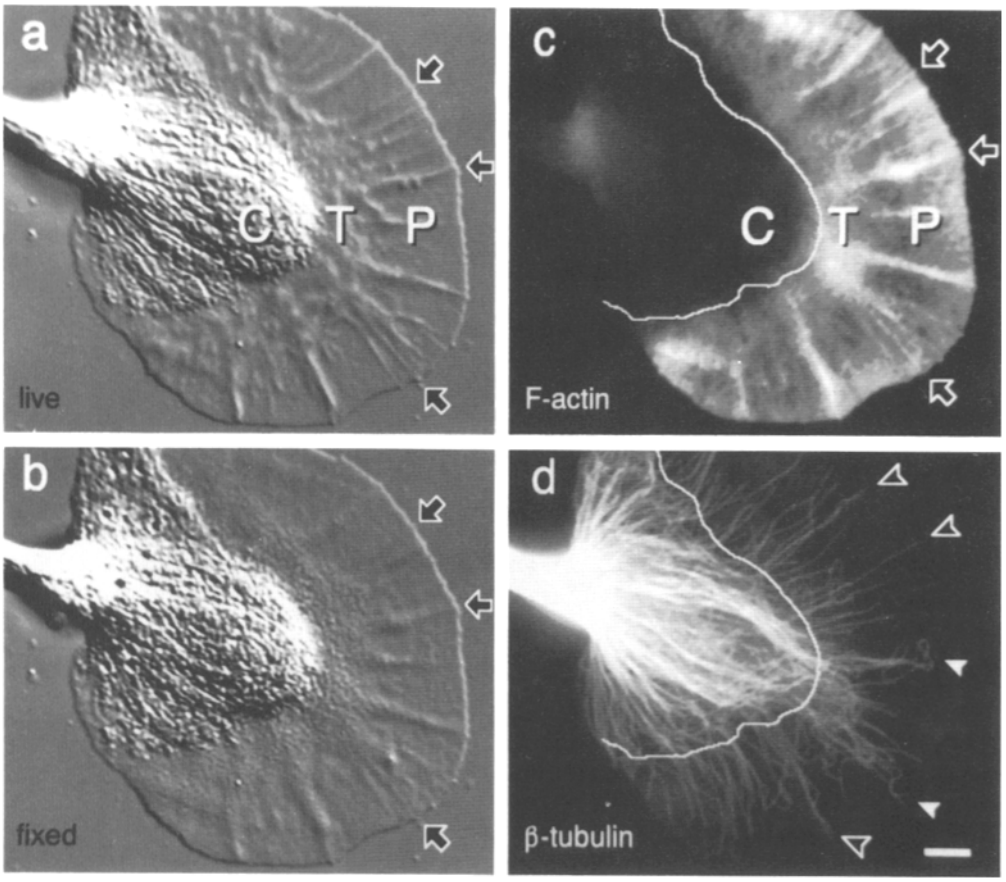

Figure 1. Cytoskeletal distributions in an acutely plated growth cone. (*a* and *b*) DIC images of a growth cone before (*a*) and after fixation (*b*). Central (*C*), peripheral (*P*), cytoplasmic domains and transition zone (*T*) are indicated. (*c*) F-actin and (*d*) microtubule distributions visualized with rhodamine-phalloidin staining and anti-β-tubulin secondary immunofluorescence, respectively. Distal margin of the C domain is marked by *white lines*. Note the radial actin bundles (*arrows*) and microtubules penetrating into the P domain (*arrowheads*). Some microtubule loops are also present (*white arrowheads*). Bar, 5 μm.

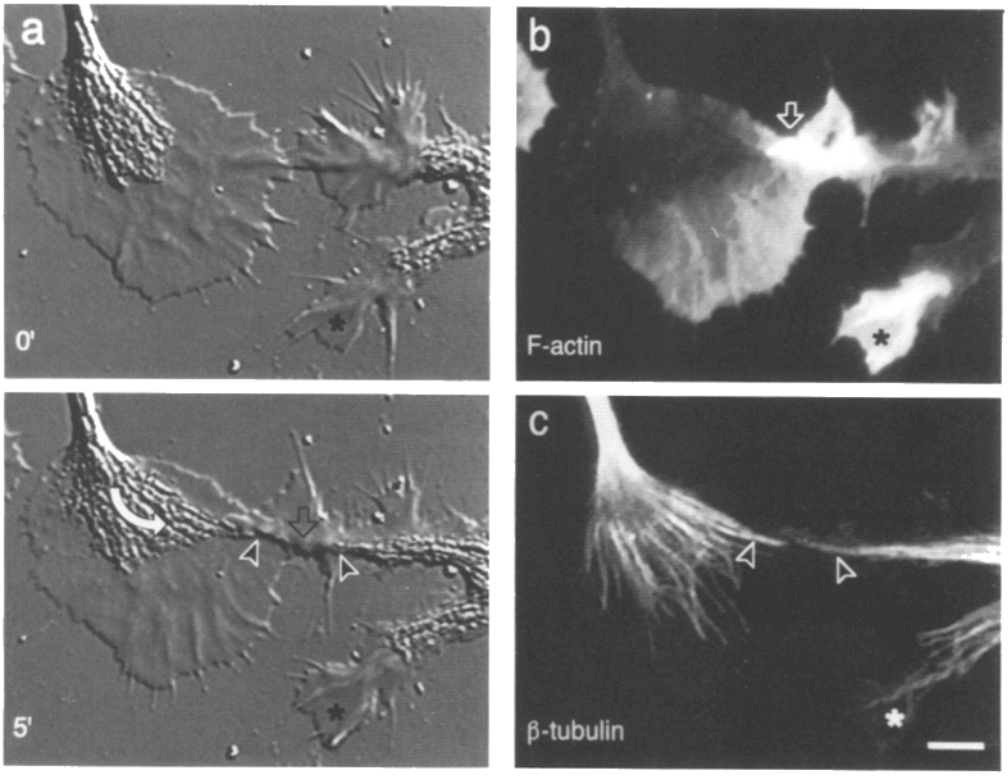

Figure 2. Remodeling during the early phase of a growth cone–target interaction. (*a*) DIC image sequence of an interaction between two growth cones from neighboring neurons. Time in minutes indicated at bottom left. After 5 min, note membrane ruffling (*open arrow*) and preferential C-domain extension (*curved arrow*) toward the contact site. (*b–c*) F-actin and tubulin localizations. Note the concentration of F-actin at contact zone (*arrow*) and the target site-specific microtubule extension. Arrowheads mark the location of the most distal organelles used to track the microtubule movement. No changes were observed in a noninteracting growth cone (*asterisks*). Bar, 5 μm.

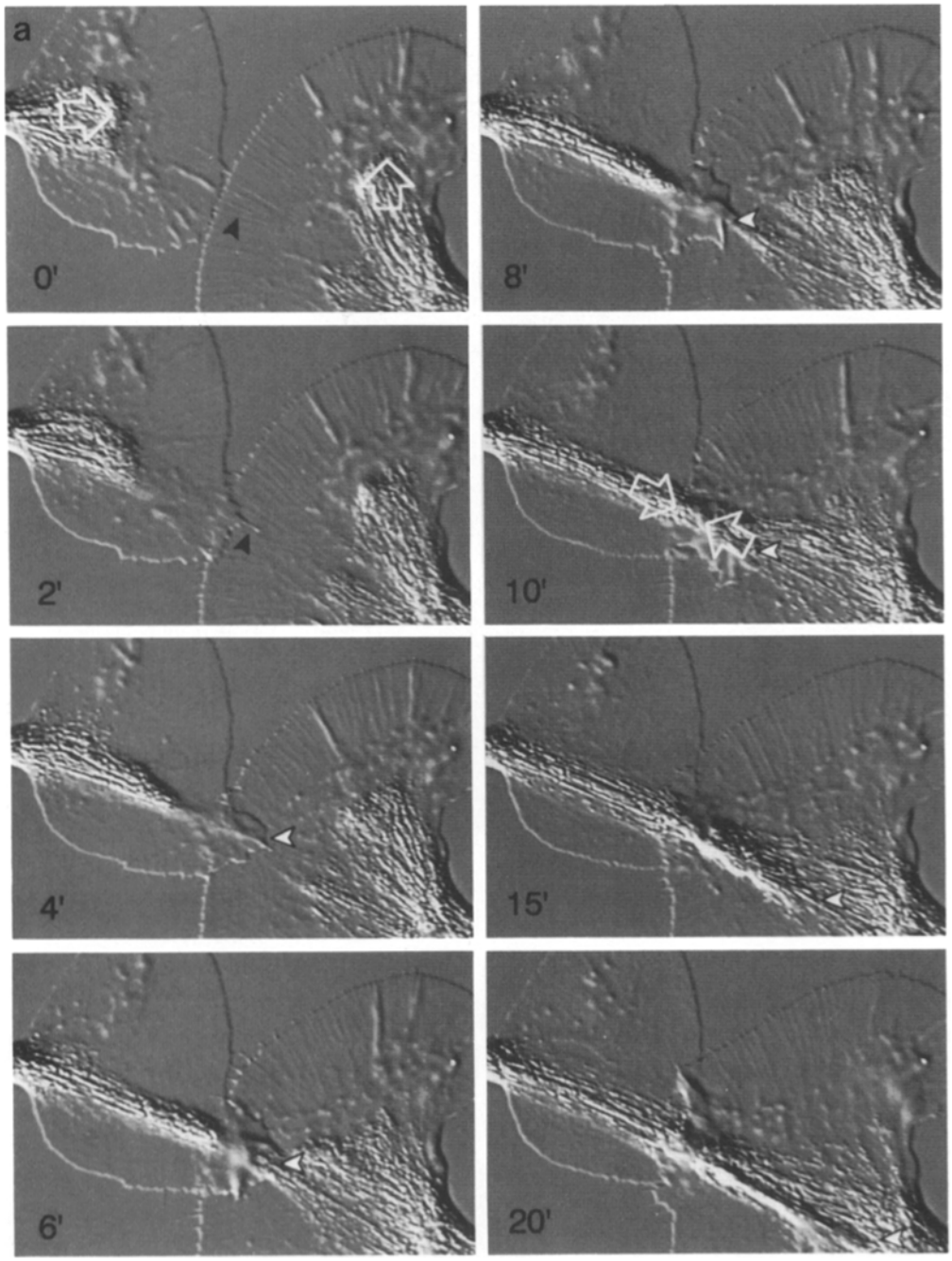

Figure 3. Remodeling during a long term growth cone–target interaction. (*a*) Video-DIC time course of a 20-min interaction, time indicated in minutes. Signs of cell coupling (stretched filopodium, *black arrowheads* at *0′–2′*) indicate initiation of this interaction, which in 10 min, reoriented the direction of growth cone outgrowth (compared *open arrows* at *0′* and *10′*). In the following 10 min (*10′–20′*), note intensive membrane ruffling proximal to the leading edge of left growth cone (*white arrowhead*). (*b–c*) F-actin and microtubule distributions corresponding to the 20-min timepoint. Note the concentration of F-actin at the distal portions of both growth cones (*arrowheads*) and the prevalence of microtubule arrays along target interaction axis (*double-headed arrow*). Inward curvature of individual off-axis microtubules (*c, white arrows*) suggests "zippering" of microtubules into the main axial bundle. Bar, 5 μm. (*d*) Kinetics of C domain advance during this growth cone–growth cone interaction.

West Grove, PA), washed with PBS, transferred to a mounting solution containing PBS supplemented with 20 mM *n*-propyl gallate (Sigma Chem. Co.) and 80% glycerol, and examined immediately for fluorescent staining. In control experiments where the tubulin primary antibody was omitted or cells were incubated with unlabeled phalloidin before exposure to fluorescent probes, there was little or no labeling observed.

Results

Microtubule and Actin Filament Distributions in Acutely Plated Growth Cones

Bag cell neurons sprouted growth cones on distal neurites within several hours after plating at room temperature on poly-L-lysine substrates. Neurite outgrowth typically progressed in a saltatory manner at rates of 0.1 ± 0.05 μm/min under these conditions (see below). Growth cone structure and cytoskeletal distributions 16 h after plating are illustrated in Fig. 1.

A growth cone typically has two cytoplasmic domains: the peripheral lamellar (*P*) domain and the central (*C*) domain. Overlapping regions between these two domains are referred to as the transition (*T*) zone (Bridgman et al., 1986; Forscher et al., 1987). The P domain (*P*, Fig. 1) consists primarily of F-actin, including radial cables (*arrows*) that coalign with filopodia and less polarized but highly cross-linked networks found between cables (cf., Lewis and Bridgman, 1992). These F-actin networks have been shown to assemble preferentially at nucleation sites along the distal growth cone margin and subsequent to assembly, cross-

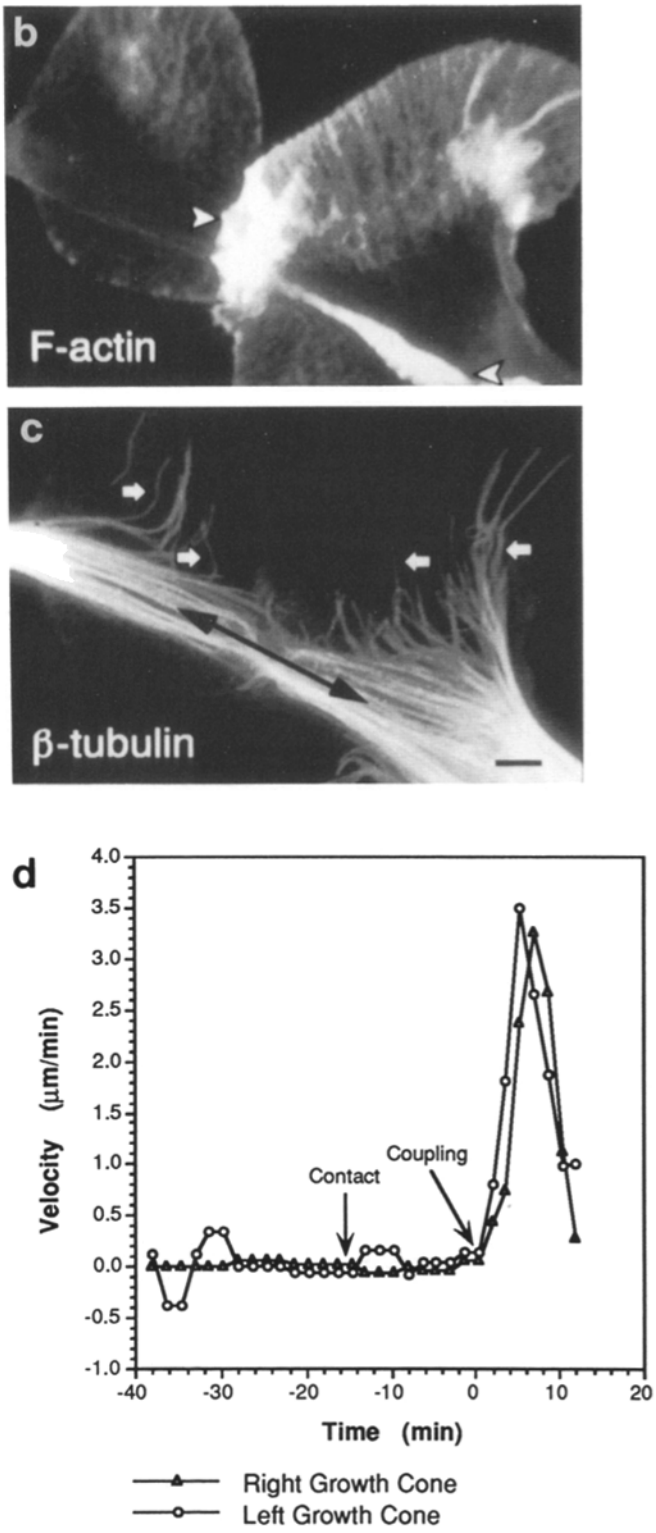

Figure 3.

linked networks move centripetally at rates of 3–6 μm/min by a mechanism that likely involves an actin-based motor(s) (Mitchison and Kirschner, 1988; Smith, 1988).

The C domain was operationally defined as the proximal portion of the growth cone characterized by organelle transport observable at the video enhanced DIC level (*C*, Fig. 1). Microtubules are the principal cytoskeletal component in the C domain, serving not only as structural elements but also as substrates for fast axonal (organelle) transport. Immunofluorescence localization revealed that microtubules were distributed throughout much of the growth cone and sometimes penetrated deeply into the P domain of these acutely plated cells (*arrowheads*). Microtubule loops (*white arrowheads*) reported by other groups to be characteristic of less motile growth cones (Tanaka and Kirschner, 1991) were also observed. Note that in the present study cells were maintained in serum-free medium at all times and interactions were studied 12–36 h after plating. This contrasts with a previous report in which growth cones were exposed to 0.5% FCS and studied 2–4 d after plating (Forscher and Smith, 1988). Under the latter conditions, microtubule density in a typical growth cone drops much more precipitously distal to the C domain boundary, and actin cables were more prominent than in these "young" growth cones. Significant overlap of microfilaments and microtubules occurs in the T zone (*T*, Fig. 1), along with active membrane ruffling characterized by lamellar protrusions in the Z-axis.

Initial Events

To promote growth cone–target interactions in vitro, individual bag cell neurons were positioned next to each other such that a single growth cone could interact with other growth cones or neurites from neighboring cells. A DIC image sequence depicting initial events during a growth cone–growth cone interaction and the corresponding cytoskeletal distributions are illustrated in Fig. 2. 16 h after plating, physical contact between these two growth cones occurred. After a lag of ~10 min, signs of cell coupling were seen which indicated the beginning of a target interaction sequence (time *0'*). During the following 5-min interval (*0'–5'*, Fig. 2 *a*), several distinct morphological changes were sequentially observed: increased membrane ruffling at the target contact site (*arrow*, *5'*), followed by a preferential extension of the C domain (*arrowheads*, *5'*) toward the same site. During this period, the C domain of the growth cone on the left projected a wedge-shaped array of organelles (*curved arrow*) toward the target growth cone on the right.

After this brief (5 min) target interaction, F-actin was already concentrated at the contact site (*arrow*, Fig. 2 *b*). The intensity of the F-actin signal measured here was greater than the sum of the signals from adjacent lamellae, suggesting that the intensification was not caused by overlapping of lamellae alone. Microtubule localization for the same field indicated that microtubule redistribution paralleled the target site directed C domain extension; note the preferential microtubule extension toward the site of F-actin concentration (*arrowheads*, Fig. 2 *c*). These and the following results also show that the presence of microtubule-based organelle transport (i.e., the location of the C domain) can be a useful marker of microtubule locations in live cells. It should be noted, however, that there are usually several μm at distal microtubule ends that are vesicle-free (segments distal to the *arrowheads*, Fig. 2, *a* and *c*). Sequential changes in organelle distribution in live cells should thus be interpreted conservatively and used as an indicator of the approximate microtubule endpoints. Finally, note that most of the microtubules in the left hand growth cone remain spread and do not appear to have reacted to the target interaction at this

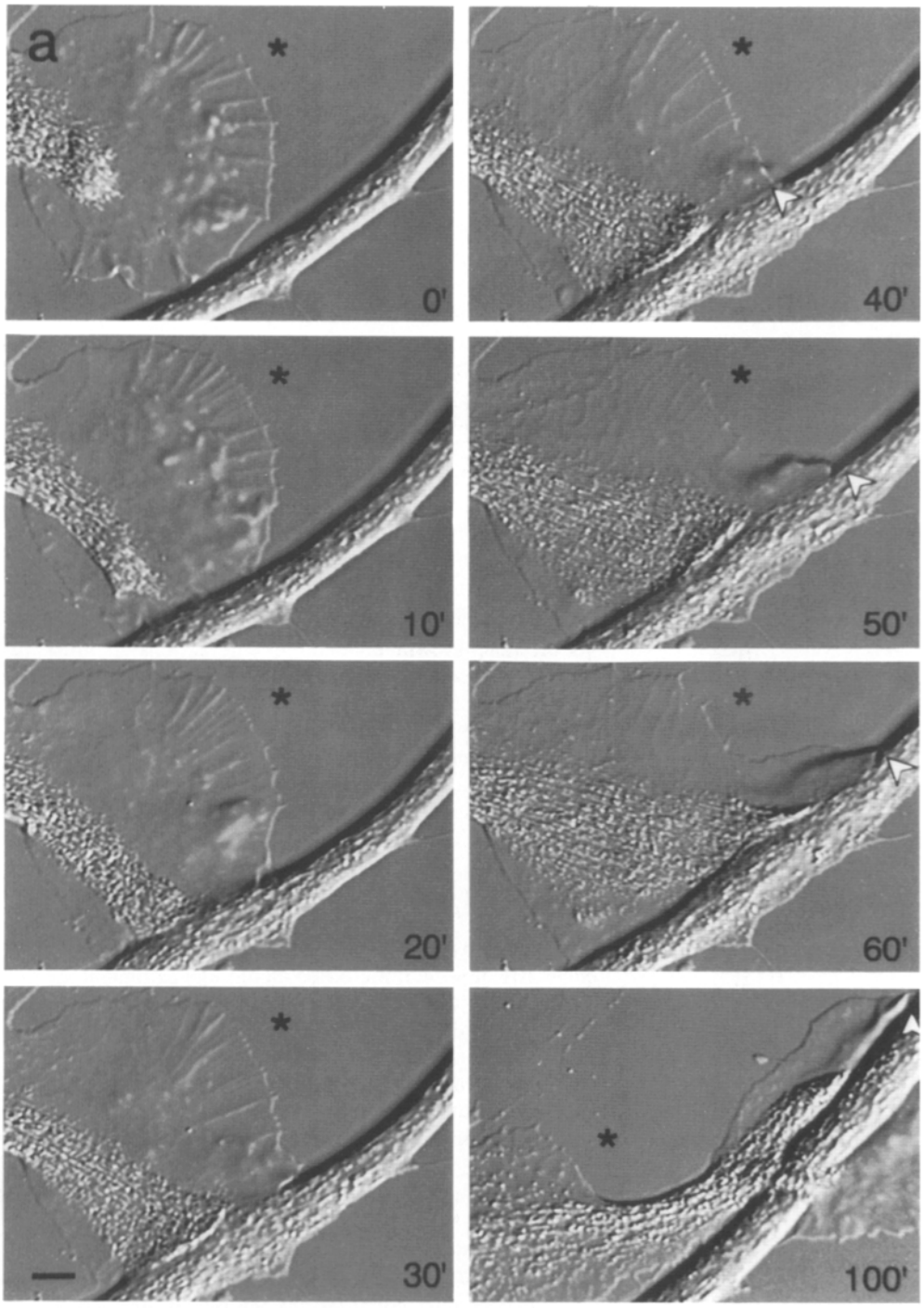

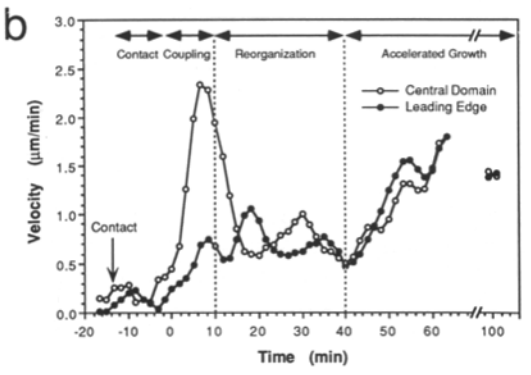

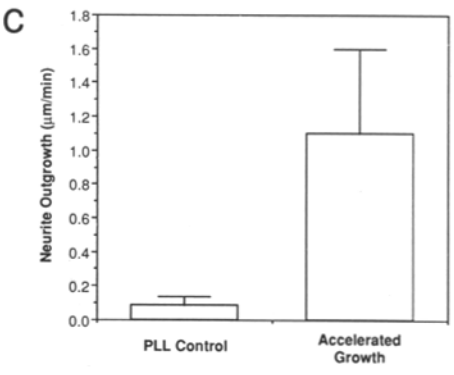

Figure 4. Growth cone–target interactions modulate neurite outgrowth. (*a*) Sequential DIC images of a growth cone–neurite interaction. Note intensive membrane ruffling at the leading edge (*arrowheads*) during fasiculated outgrowth. Asterisks label a reference point since the field was moved in the last panel to follow the rapidly migrating growth cone. Bar, 5 μm. (*b*) Kinetics of growth cone migration plotted over time for central domain (*open symbols*) and leading edge extension (*closed symbols*). Key events and functional phases of the interaction are indicated. (*c*) Control outgrowth rates on poly-L-lysine substrate vs. fasciculated outgrowth rates along native target substrates. Mean ± SEM values are shown. Control outgrowth: 0.09 ± 0.05 μm/min from 31 measurement of 12 growth cones. Fasciculated outgrowth: 1.10 ± 0.50 μm/min from 41 measurements of 10 interactions.

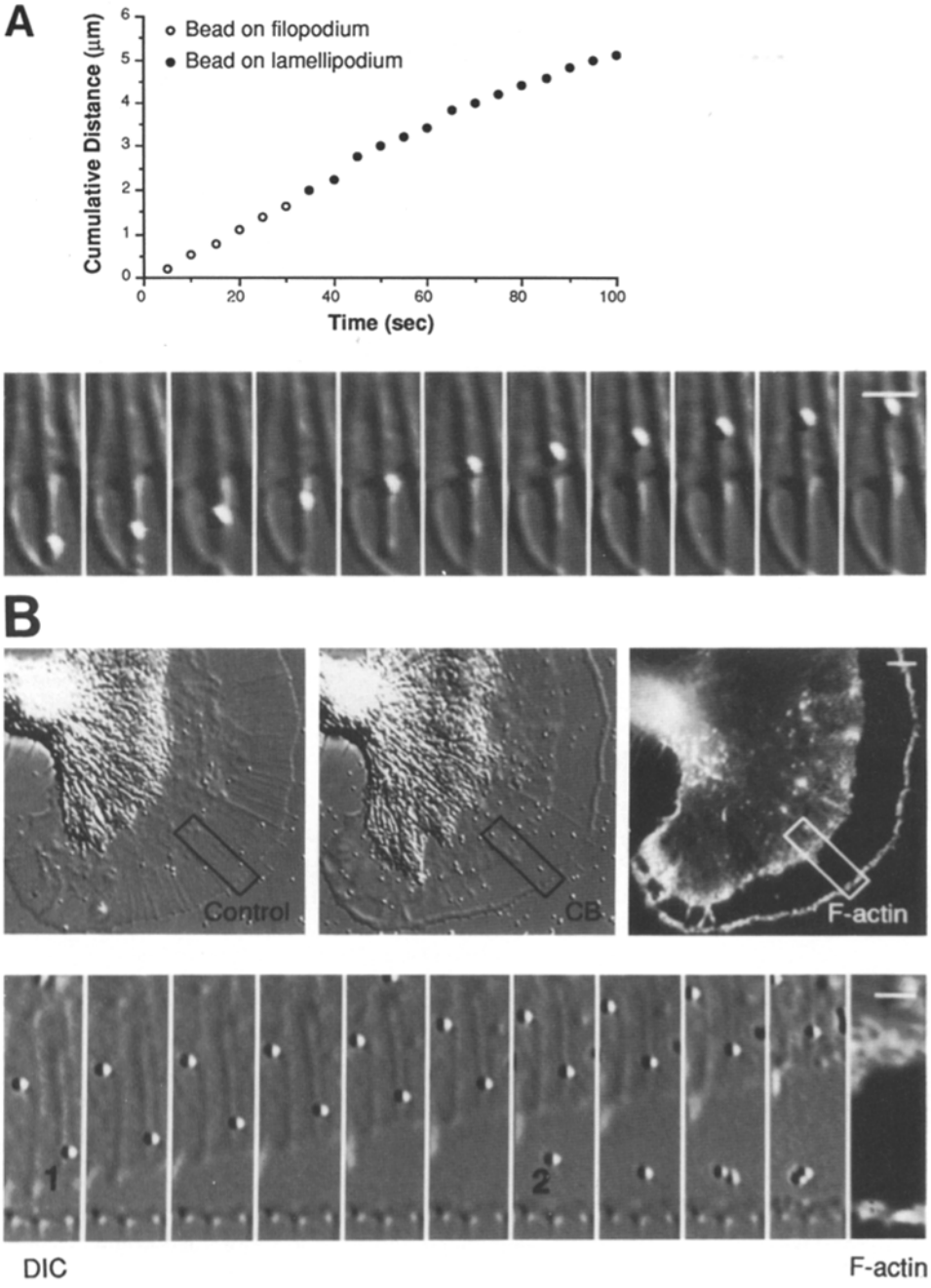

Figure 5. Pseudotarget translocation on the growth cone surface is F-actin dependent. (*A*) Retrograde translocation sequence of a 200-nm positively charged bead on the surface of a growth cone. Frames in montage are separated by 10-s intervals; cumulative bead displacement is plotted as a function of time. Note that transport rate down the filopodium (*open circles*) is the same as that observed on the lamella (*closed circles*). (*B*) Bead transport results from coupling to underlying F-actin flow. A pulse of cytochalasin B (*CB*) caused an F-actin free gap to form along the leading edge as evidenced by corresponding rhodamine-phalloidin staining (*F-actin*). Frames in montage (10-s intervals) show bead dynamics in the area of interest during *CB* treatment. Bead *1* attached before the drug application and continued to move at the same rate as the receding F-actin network. Bead *2* bound distal to the receding F-actin matrix and exhibited brownian motion during the observation period. Bars, 2 and 5 μm for montage panels and growth cone images, respectively.

early time point. This is in marked contrast to effects seen after more prolonged interactions (Fig. 3). Significant structural changes were not observed in an adjacent growth cone not directly involved in this interaction (*asterisks*, Fig. 2).

Later Events

Effects of a longer growth cone–target interaction are illustrated in Fig. 3. During a 30-min period of observation before contact, both growth cones slowly advanced at ~0.05 μm/min on a poly-L-lysine substrate. A marked projection of the bulk of the C domain (*open arrows* at *0′*, Fig. 3 *a*) typically indicated the direction of growth cone migration.

15 min after the first discernible contact, signs indicating mechanical coupling between the interacting growth cones were observed (marked here as time *0′*), as evidenced by the stretched filopodium of the left growth cone apparent on the dorsal lamella of the right growth cone (*black arrowheads* at *0′–2′*, Fig. 3 *a*). During the following 10 min, radial actin cables over the target contact region gradually disappeared and transformed into intensive ruffling (*white arrowheads*); and then the C domains of both growth cones extended rapidly toward each other (*open arrows* at *10′*, Fig. 3 *a*). Using regions of directed organelle transport and membrane ruffling as rough indicators of microtubule and F-actin localization, respectively, we observed a temporal sequence where local F-actin reorganization always preceded anterograde microtubule movement.

This type of interaction often resulted in net reorientation of neurite outgrowth. Specifically, note that the growth cones

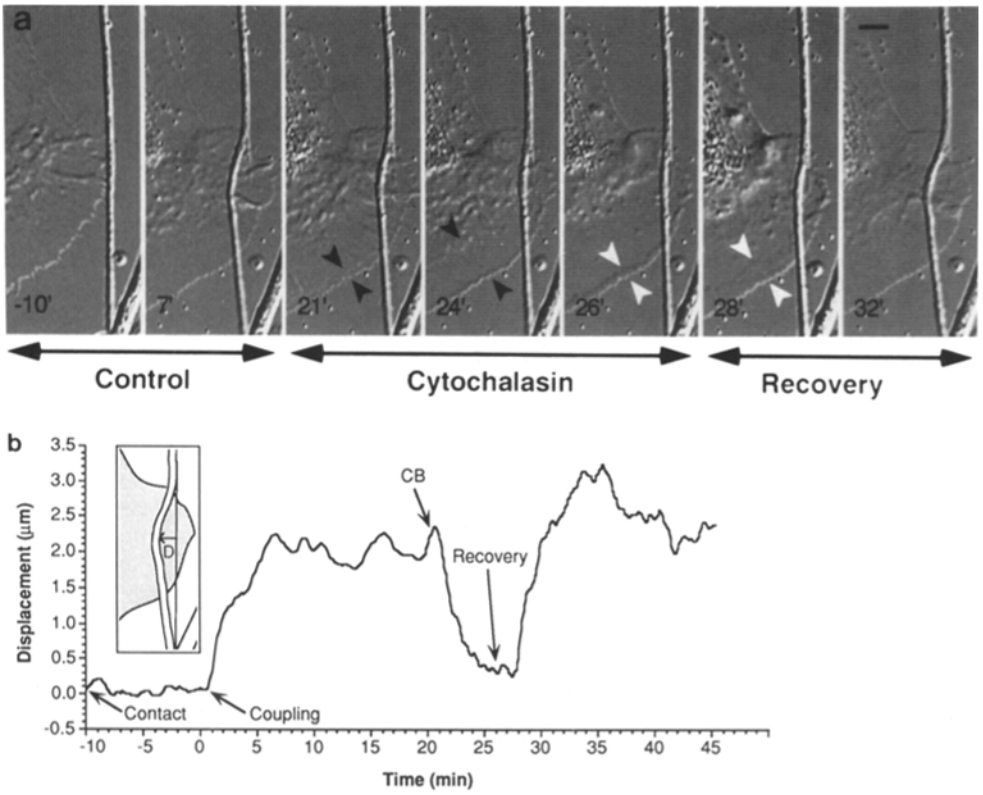

Figure 6. Target cell coupling is F-actin dependent. (*a*) Time course of an interaction between a growth cone and a semi-compliant neurite in response to cytochalasin treatment. Cell coupling is manifested here as neurite bending. This bending force was reversibly released by cytochalasin B treatment. Note gap formation between the leading edge and the receding F-actin network during onset of drug effects (*black arrowheads*) and band of newly assembled F-actin along leading edge during initial recovery phase (*white arrowheads*). Bar, 5 μm. (*b*) Kinetics of neurite bending. Neurite displacement is plotted as a function of time. Key events indicated correspond to those discussed in text: *CB* addition at *20'*, *Recovery* at *25'*.

in Fig. 3 *a* turned a total of ~45 degrees during realignment along the interaction axis (compare *open arrows* at *0'* and *10'*). In the next 10 min (*10'–20'*), the originally well spread C domains were further rearranged and consolidated along the target interaction axis. While the right growth cone remained relatively stationary during this period, the left growth cone rapidly advanced (at ~1.5 μm/min), with active membrane ruffling associated with its leading edge (*white arrowheads*), over the dorsal surface of the right growth cone.

Cytoskeletal localizations were then assessed for this interaction at the 20-min time point. Distinct accumulation of F-actin was found coincident with the zone of intensive membrane ruffling near the target site (*arrowhead*, Fig. 3 *b*). The degree of F-actin accumulation had increased relative to that observed after a shorter 5 min interaction (Fig. 2 *b*). Furthermore, the actin filament density was lower proximal to the target site, consistent with anterograde movement or depletion of F-actin from these areas. Most of the microtubules had extended enough to bridge the contact zone, forming bundled arrays aligned along the interaction axis (*double-headed arrow*, Fig. 3 *c*). Only a few microtubules remained spread and curved away from the main axial bundles (*arrows*). C domain extension rates during the target interaction in Fig. 3 *a* are plotted as a function of time in Fig. 3 *d*. There was a 15-min delay between initial physical contact and signs of neuronal coupling (*time 0'*). The maximum rates of C domain extension were 3.5 and 3.1 μm/min for the growth cone on the left and right, respectively.

During growth cone–growth cone interactions, accurate tracking of the C domain and leading edge became difficult when the interacting components overlapped. We therefore studied growth cone movements on neurites to obtain a clearer analysis of outgrowth kinetics. The DIC sequence of one such interaction is demonstrated in Fig. 4 *a*, and the rate of advance of the C domain (*open circles*) and the leading edge (*closed circles*) are plotted over time in Fig. 4 *b*. Based on the growth cone dynamics, we divided the interaction sequence into four functional phases (Fig. 4 *b*): a contact phase (*−13'–0'*), between initial contact and cell coupling; a coupling phase (*0'–10'*), characterized by target site specific ruffling and rapid C domain extension; a reorganization phase (*10'–40'*), characterized by intensive cytoskeletal remodeling but slow overall outgrowth; and an accelerated growth phase (*40'–100'*), where the growth cone migrated along the native target substrate in a manner analogous to axonal fasciculation (Goodman et al., 1984; Dodd and Jessell, 1988).

During the accelerated growth phase, the growth cones typically moved partially or fully off the poly-L-lysine substrate onto the neuronal membrane of the target cell. Interestingly, rates of neurite outgrowth increased about one order of magnitude by the time this transition was complete and the higher outgrowth rates were subsequently maintained. The average rates of neurite outgrowth after fasciculation are compared to those observed on a poly-L-lysine substrate in Fig. 4 *c*. Note also that rates of both the C domain and the leading edge advance increased in parallel during the accelerated growth period and stabilized at ~1.4 μm/min after ~1 h (*100'* time point, Fig. 4 *b*). Since the C domain advanced at a rate comparable to the leading edge, the P domain maintained a relatively constant width in all but the coupling phase. Intense ruffling was always observed at the distal edge of growth cones during accelerated outgrowth (*arrowheads*, Fig. 4 *a*).

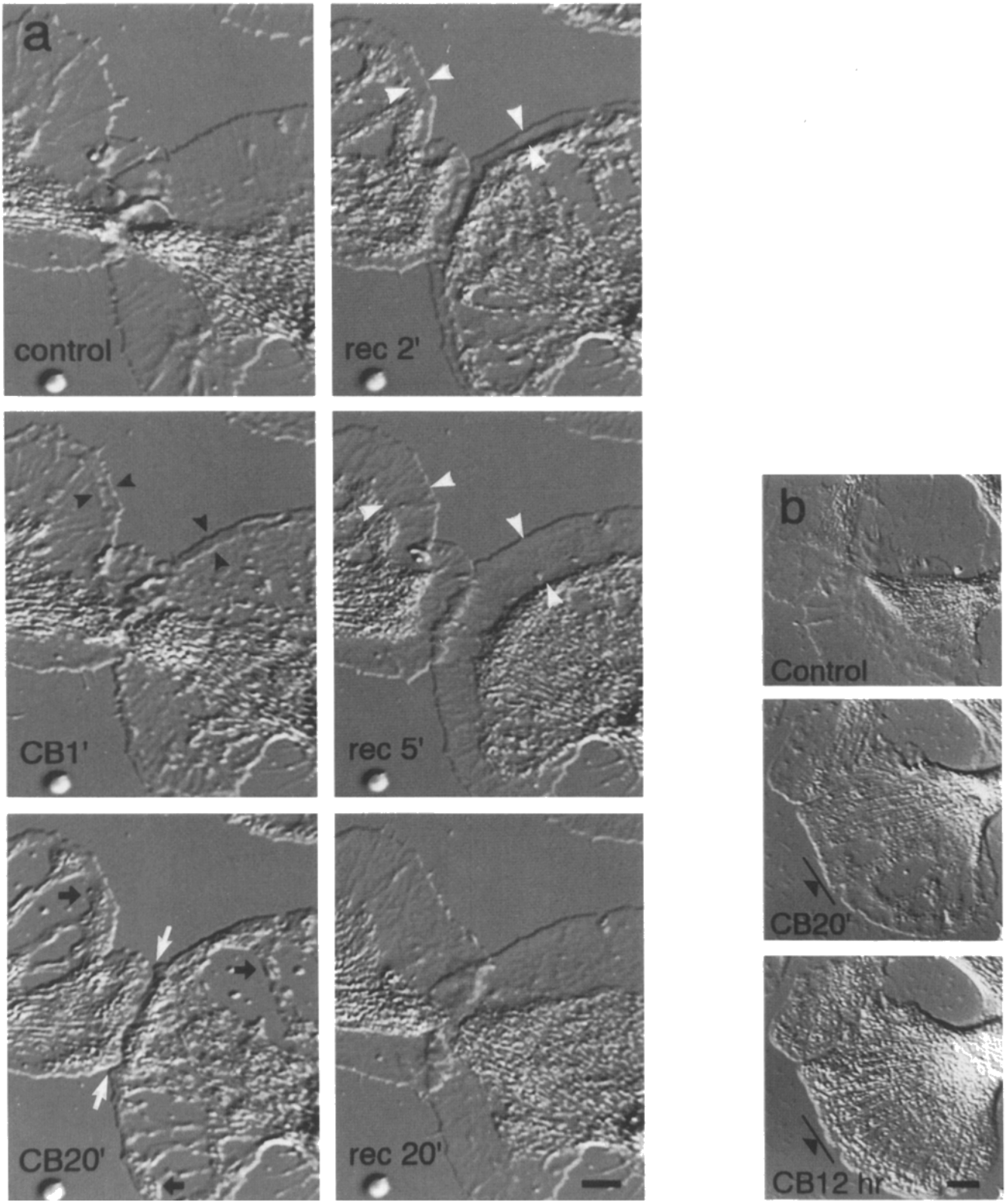

Figure 7. Target induced remodeling events are F-actin dependent. (*a*) Sequential DIC images of an ongoing growth cone-target interaction briefly treated with cytochalasin B (*CB*). Note the breakaway (*black arrowheads*) of the F-actin network after 1 min of *CB* exposure. Microtubules and C domain components then randomly pervaded into the areas devoid of actin matrix (*black arrows*). Note that *CB* treatment essentially eliminated growth cone reorientation induced by the target contact (*CB20'*). During recovery, dense actin matrix reappeared and grew centripetally (*white arrowheads, rec 2'–5'*). The target interaction then resumed at the original site (*rec 20'*). (*b*) Chronic *CB* effects. A target interaction was inhibited by treatment with *CB* (*CB20'*), and then maintained in the continual presence of the drug overnight (*CB12 hr*). There is no net growth cone advance (bars represent a reference frame) during the chronic CB exposure. Bar, 5 μm.

Cytomechanics of Pseudotarget vs. Real Target Interactions

The growth cone–target interactions described above are complex. We therefore used derivatized microparticle pseudotargets as a tool to investigate the possible underlying mechanisms of real target events. Positively charged polystyrene beads are typically transported at constant rates from the lamella edge across the P domain and into the transition zone (see also Forscher and Smith, 1990, for a preliminary description of this phenomenon). This bead movement persists in the most distal portions of filopodia. As shown in Fig. 5 *a*, after adhering to the distal tip, this 200-nm bead moved down the length of the filopodium onto the surface of the lamella at a constant rate. Cumulative displacement of the bead is plotted as a function of time in Fig. 5 *a*. Note that bead velocity remained relatively constant (~3 μm/min) at all times, even as the bead crossed the boundary between the filopodium (*open circles*) and the lamellipodium (*closed circles*). Bead rates in a given growth cone were similar for bead movements along or in between the radial actin cables. Fig. 5 *b* provides evidence that the bead movement likely results from mechanical coupling to the underlying F-actin flow. A pulse of cytochalasin B was applied when beads were undergoing retrograde transport at 4.4 ± 0.09 μm/min. The treatment resulted in formation of a typical F-actin free gap between the leading edge and receding F-actin networks as evidenced by rhodamine-phalloidin staining (Fig. 5 *b*). Those beads attached to the membrane before drug application (bead *1*) were continuously transported at 4.52 ± 0.17 μm/min with the receding F-actin matrix (which moved at 4.59 ± 0.17 μm/min), while beads that landed after drug exposure and bound to the F-actin free zone (bead *2*) moved randomly. Only after washout of cytochalasin, were beads directionally transported again by the recovered F-actin flow (data not shown, but see Forscher and Smith, 1990).

To test if similar transport mechanisms could account for target cell coupling events, the sensitivity of neurite bending to cytochalasin exposure (Fig. 6) was compared with the movement of bead pseudotargets after the same treatment (Fig. 5). The neurite coupled to the interacting growth cone was bent toward the C domain (*Control*, Fig. 6 *a*). This neurite bending force was reversibly inhibited by adding cytochalasin. When the F-actin free gap (*black arrowheads*) moved past the site of neurite contact, tension appeared to be released, and the neurite straightened and relaxed toward the leading edge (*Cytochalasin*, Fig. 6 *a*). Upon washout of cytochalasin, a dense F-actin matrix reappeared, primarily from the growth cone margin, and widened centripetally (*white arrowheads*). Deflection of the neurite was again observed as the F-actin matrix began to move beneath it (*28* min). After 4 min of recovery in control saline, the forces associated with neurite bending appeared to have been restored to pretreatment levels (cf., *7* and *32* min). Neurite displacement as a function of time is plotted in Fig. 6 *b*. Displacement rates during initial coupling and recovery from cytochalasin treatment were ~2.76 μm/min and 3.09 μm/min, respectively, similar to typical rates of retrograde F-actin flow and bead movement.

Microtubule Guidance Is Disrupted by Cytochalasin

To investigate the role of actin filament dynamics in target site–directed microtubule extension, we treated interacting growth cones with cytochalasin B for various periods of time. As shown in Fig. 7 *a*, the C domain extension toward the contact zone was observed 10 min after growth cone coupling (*control*). Cytochalasin B was then rapidly perfused into the flow cell. After one minute of drug treatment, a gap formed along the leading edge (*black arrowheads* at *CB1'*, Fig. 7 *a*) indicating continued retrograde F-actin movement similar to that observed above (Figs. *5* and *6*). Membrane ruffling at the target site was immediately inhibited by the drug and overlapping lamellae retracted to where they adhered to the poly-L-lysine substrate (*white arrows* at *CB 20'*). Secondary to these initial effects, the C domain began rapid distal spreading into the area initially occupied by actin filaments (*black arrows* at *CB20'*).

After drug washout, a dense F-actin matrix appeared along the leading edge of each growth cone and a typical recovery occurred accompanied by centripetal movement of C domain elements (*white arrowheads* at *rec 2'–5'*, Fig. 7 *a*). After 5 min of recovery, both P and C domain boundaries were transiently restored to positions roughly corresponding to precontact localizations. Interestingly, target interactions then resumed at the point of original contact (*rec 20'*, Fig. 7 *a*). There was essentially no delay in extension of the C domain; this differs from a naive growth cone–target interaction where a 15–30-min delay is typically observed between initial contact and manifestations of cell coupling (cf. Fig. 3). Even after 2 h of cytochalasin treatment, drug washout resulted in resumption of target interactions at the original site of contact (data not shown).

After longer cytochalasin treatments, the randomization of microtubule extension is more evident. This is illustrated in Fig. 7 *b* which shows two growth cones before, 20 min and 12 h after cytochalasin B treatment. During chronic cytochalasin exposure, the C domain progressively occupied the full extent of the former P domain and no net outgrowth of the growth cone was observed.

Neuronal Branching: Competition for the Microtubule Pool

Neurite branching often resulted from competitive interactions between growth cones (Fig. 8). In this example, growth cone *1* initially interacted with growth cone *2* (*time 0'*) in a typical structural reorganization sequence that lasted ~20 min, at which time growth cone *3* initiated a competitive interaction. The competitive interaction resulted in partitioning of the C domain of growth cone 1 (*branched arrow* at *41'*) between the growth cones *2* (*white arrows*) and *3* (*black arrows*). In 4 out of 5 cases where competitive interactions were observed, neurite branching resulted. In the fifth case, however, one growth cone was "dominant" and was able to recruit the entire microtubule pool to its interaction axis (data not shown).

Specificity of Interactions

There were two classes of cells in this primary culture system: bag cell neurons and glia-like support cells. Glia-like cells were smaller than neurons (10 μm in diameter compared to 50–70 μm of neurons), and did not have processes or growth cones. However, these cells generated peripheral lamellae that exhibited comparable retrograde F-actin flow

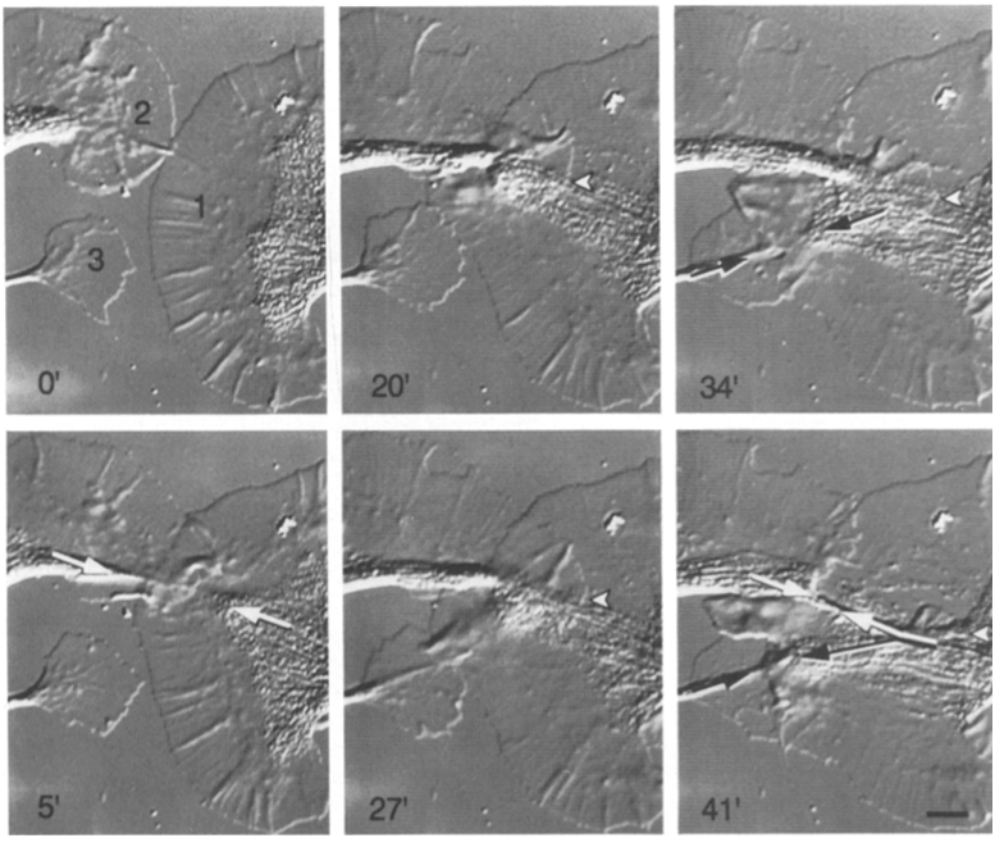

Figure 8. Target competition for the microtubule/organelle pool. DIC sequence of a competitive interaction. Growth cone *1* first interacted with growth cone *2* (*white arrows*). After 20 min, another interaction was initiated between growth cone *1* and *3* (*black arrows*), while growth cone *2* continued to migrate on top of growth cone *1* (*arrowheads*). This competitive interaction resulted in partitioning of the microtubule/organelle pool of the shared growth cone *1* (*branched arrow*). Bar, 5 μm.

rates. In several long term observations where growth cones physically contacted these cells, no signs of cell coupling or cytoskeletal remodeling were observed (data not shown). No increase of ruffling was noted at the contact site and the local density of F-actin was not higher than the sum of the signals from individual cells. Thus, the series of events described above appear to be cell specific, and indicate that essential target recognition processes may underlie the processes described.

Discussion

A Primary Role for Actin Filaments in Growth Cone Steering

Previous work addressing the mechanism of growth cone guidance in pioneer neurons of grasshopper embryos suggested that microfilament dynamics were important for growth cone steering (Bentley and Toroian-Raymond, 1986), and a later study presented evidence that steering could be mediated by single filopodial contacts (O'Connor et al., 1990). In a subsequent report, however, it was proposed that selective retention and invasion of microtubules may alternatively be of key importance in the steering process (Sabry et al., 1991). In the present study, we have focused on possible interactions between actin filaments and microtubules during growth cone–target encounters in an attempt to clarify the role played by each cytoskeletal element.

To summarize, our observations suggest that actin based motility and polymer dynamics play a primary role in both initiating and articulating growth cone steering events for the following reasons: First, growth cone filopodia, which consist of relatively parallel bundles of F-actin (Lewis and Bridgman, 1992; Smith, 1988), always initiated interactions, thereby determining the target interaction axis, and additionally, future microtubule movements and localization. Second, during an interaction, microtubules initially arranged in fanned out arrays became aligned with the interaction axis and extended specifically toward the site of F-actin accumulation (e.g., Fig. 3). Third, cytochalasin treatments resulted in immediate randomization of microtubule extension; recovery from cytochalasin resulted in resumption of target site–directed movement of microtubules (Fig. 7). Finally, a variety of objects including polystyrene beads, small caliber neurites, large neurites, and other growth cones were found to interact with actin networks undergoing retrograde flux, eliciting a variety of effects on growth cone structure. These effects could be accounted for by considering the degree of target compliance by a mechanism which will be considered further below.

The directed microtubule movements we observe during a typical growth cone–target interaction probably involve several contemporaneous processes including: (*a*) microtubule assembly and disassembly (dynamics); (*b*) active microtubule telescoping (Lasek, 1986; Shpetner and Vallee, 1989); and (*c*) microtubule interactions with moving actin networks. Further experiments using fluorescent tubulin analogs to directly assess microtubule dynamics are needed to address processes 1–2; however, some comments can be made regarding microfilament associated microtubule move-

ments. During the course of a typical interaction microtubules appeared to be swept progressively into axial alignment (parallel to the target interaction axis) as evidenced by observation of organelles undergoing microtubule-based transport, and examination of microtubules fixed and stained after target interactions were well underway (e.g., Fig 3 *c*). Off axis microtubules typically had curvilinear profiles with their convex aspect facing toward the target site, suggesting that fixation occurred as the microtubules were being pulled or "zippered" laterally toward the target contact area. Visual observation of DIC time-lapse records strongly suggested that over time cytoplasmic material was being depleted from areas lateral and proximal to the contact zone. A progressive decrease in F-actin levels and retrograde flow occurred in parallel with the cytoplasmic depletion in these areas. These observations suggest microtubules become aligned along the target interaction axis via association with actin filaments accumulating at the contact site. Note that F-actin accumulation might occur by one of several mechanisms that remain to be elucidated: (*a*) formation of specific flow retarding membrane-cytoskeletal connections or adhesion complexes, (*b*) increased actin assembly secondary to target contact, or (*c*) active recruitment (pulling) of already formed filaments into the contact zone.

We also found a correlation between microtubule distribution and neurite outgrowth rate: microtubules in stationary growth cones tended to be splayed out and sometimes formed loops (Fig. 1), whereas microtubules in rapidly migrating growth cones tended to be bundled into linear arrays (Fig. 3). Our results are consistent with previous observations of microtubule dynamics in growth cones (Tanaka and Kirschner, 1991) where microtubules were splayed out in slowly advancing growth cones but formed linear bundles when the rate of advance exceeded the rate of microtubule translocation. The inward curvature of the microtubules toward the target interaction axis mentioned above (Fig. 3 *c*) is also consistent with a bundling mechanism involving a proximal to distal zippering as suggested by Tanaka and Kirschner (1991) after observations of microtubule movements during growth cone turning.

Many cell functions in both neuronal (Dennerll et al., 1989; Letourneau et al., 1987; Marsh and Letourneau, 1984) and nonneuronal (Danowski, 1989; Euteneuer and Schliwa, 1985; Euteneuer and Schliwa, 1992) cells appear to rely on coordinated interactions between the microfilament and microtubule systems. Our results also point to the presence of strong modulatory effects exerted by actin filaments on microtubule localization, specifically with regard to target site–directed microtubule guidance. Whether these effects involve direct (Schliwa and Van Blerkom, 1981) or indirect (Griffith and Pollard, 1978; Selden and Pollard, 1983; Goslin et al., 1989; Morales and Fifkova, 1989; Correas et al., 1990) molecular interactions, active participation of molecular motors, or result from alterations in microtubule dynamics remains to be determined.

Lamellipodia Dynamics

The interactions described in Results involve complex cytological transformations. To address potential underlying mechanisms, we will present a model of lamellar motility, and then interpret our current observations within the context of the model. Fig. 9 *a* is a cross section of a motile lamellipodium. Lamellar F-actin is depicted as a more or less isotropic matrix of cross-linked filaments reflecting recent ultrastructural studies suggesting at least 30% of the lamellar actin filaments do not have their barbed ends facing the distal cell margin (Lewis and Bridgman, 1992). F-actin has previously been shown to be assembled primarily at nucleation sites along the leading edge (Forscher and Smith, 1988); in addition, we show newly assembled filaments being released and cross-linked into networks (*curved arrows*) reflecting recent findings by Theriot and Mitchison (1991).

The assembled F-actin matrix moves centripetally at a rate of R_{flow} which is typically 3–6 μm/min in *Aplysia* growth cones. An actin-based motor(s) has been hypothesized to drive this movement because residual F-actin flow persists (albeit transiently) at about the same rate even after actin assembly has been inhibited (cf., Fig. 5; Forscher and Smith, 1988; Smith, 1988). The identity and localization of this putative myosin has not yet been clearly demonstrated (Bridgman and Dailey, 1989; Letourneau and Shattuck, 1989; Miller et al., 1992; Cheney and Mooseker, 1992); however, the mechanoenzyme is likely bound to a domain that is physically stable relative to the F-actin networks that are being translocated. In previous models, the "mystery motor" has been depicted as anchored to the substrate (Smith, 1988) or to a membrane-cytoskeletal matrix (Mitchison and Kirschner, 1988). A microtubule associated F-actin motor location might also be effective given the interactions reported here. Although myosins do not typically colocalize with microtubules, the notion of crossover between microfilament and microtubule based motor systems is not entirely without precedent given recent reports of single organelles exhibiting directed transport on both cytoskeletal substrates (Kuznetsov et al., 1992). The mixed polarity of actin filaments demonstrated by Lewis and Bridgman, (1992) also raises intriguing mechanistic questions regarding generation of the polarized force that drives retrograde F-actin flow.

Movement of the F-actin matrix is depicted as a steady state resulting from superimposition of three distinct kinetic processes: (1) the rate of net actin assembly (R_+) along the leading edge, (2) the rate of net actin disassembly in the T zone (R_-), and (3) the rate of retrograde actin flow (R_{flow}). In a steady state where $R_{flow} = R_+ = R_-$, the system would exhibit retrograde F-actin flow and essentially no leading edge advance, as exemplified by growth cones observed before interactions on an adhesive poly-L-lysine substrate. Conditions tending to slow the retrograde actin flow, such as indirect F-actin linkage to the substrate via adhesion complexes (*closed ovals*), would be growth promoting since the net rate of growth cone advance is equal to the net assembly rate less the retrograde flow rate, i.e., $R_{growth} = R_+ - R_{flow}$. Note that this model predicts that under favorable conditions, the maximal rate of growth cone advance would approach a limiting rate of R_+. This indeed appears to be the case in rapidly migrating cells, where the rate of leading edge (and cell) advance has been shown to be about equal to the rate of actin filament assembly (Theriot and Mitchison, 1991).

Surface markers such as extracellularly applied beads (Fig. 5) or semicompliant native targets such as the neurite in Fig. 6 appear to become coupled to actin networks through transmembrane protein complexes (Fig. 9 *a*, *pseu-*

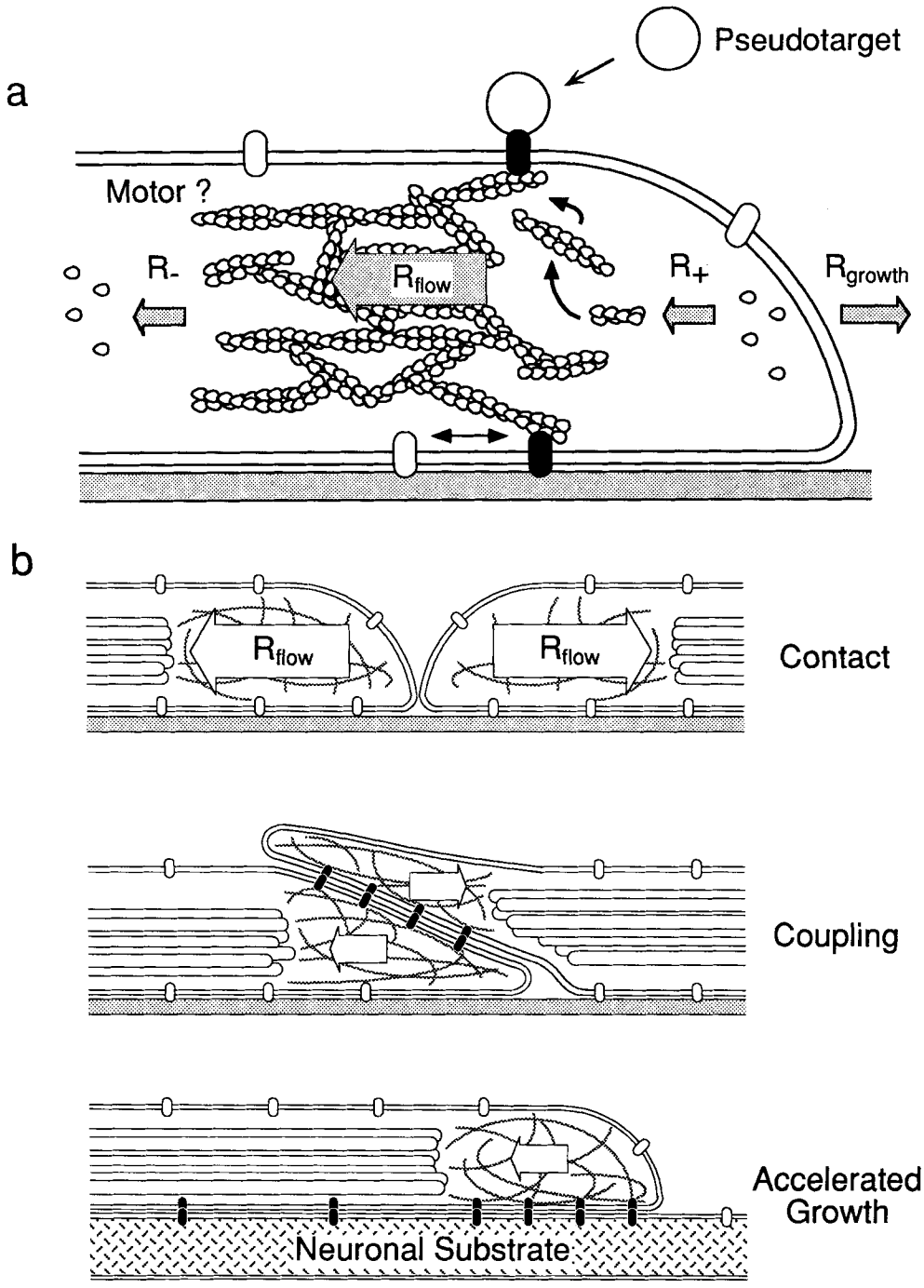

Figure 9. A model of growth cone–target interactions. (*a*) A longitudinal section through the growth cone P domain. The rate of leading edge advance (R_{growth}) depends on the relative rates of net actin filament assembly (R_+) and retrograde network flow (R_{flow}) such that $R_{growth} = R_+ - R_{flow}$. The net F-actin disassembly rate (R_-) is assumed to be constant and about equal to R_+. Oval symbols indicate putative adhesion proteins before (*open*) and after (*closed*) linkage to intracellular F-actin. Factors that promote actin filament–substrate coupling (*double-headed arrow*) tend to decrease R_{flow} and thus promote growth. Beads (*pseudotarget*) applied to the membrane surface can also become coupled to the F-actin flow but will not affect R_{growth} because they are compliant. Molecular motor(s) driving flow are indicated by *Motor?*, since their identity and localization is not known. (*b*) A target interaction may involve cell *contact*, followed by gradual accumulation of adhesion proteins (*closed ovals*) leading to intercellular F-actin *coupling* and retardation of the retrograde F-actin flow (*smaller arrows*). A decrease in R_{flow} promotes both microtubule extension and maintenance of *accelerated growth* on native neuronal substrates.

dotarget) and are thus displaced along with the retrograde flow (cf., Sheetz et al., 1989). Flow-coupled beads may therefore be good markers for intracellular F-actin movement in *Aplysia* growth cones because they move at the same rate as bulk F-actin visualized with rhodamine phalloidin after brief cytochalasin treatments (Fig. 5; see also Forscher and Smith, 1990). These results suggest a single kinetic domain dominates the retrograde flow in these lamellae. In other studies, beads moving on the membrane surface of 3T3 cells were reported to move about three times faster than photoactivated resorufin-actin marks (Theriot and Mitchison, 1992) and pinocytotic vacuoles have been reported to move at faster rates than particulate surface markers (Abercrombie et al., 1970). To address the issue of potential multiple kinetic domains raised by these reports, experiments are currently being done to directly compare the kinetics of labeled F-actin and membrane-bound bead movements in *Aplysia* growth cones. Note that in the current study, care was taken to work under conditions that limited possible kinetic complications introduced by bead-evoked actin assembly and accompanying motility as recently reported (Forscher et al., 1992).

Target Interaction Event Sequence

How can the sequence of events during a successful target

interaction be accounted for by this steady state model of lamellipodial dynamics? As illustrated in Fig. 4 *b* and schematically in Fig. 9 *b*, a typical growth cone–target interaction can be divided into four distinct phases: 1) contact, 2) coupling, 3) reorganization, and 4) accelerated growth. Before encountering a target, growth cones typically exhibit a robust and spatially uniform pattern of retrograde F-actin flow and microtubules are more or less relegated to the C domain. After initial physical contact with a target (Fig. 9 *b*), there was usually a 15–30-min delay before any observable signs of cell coupling between the interacting neurons. During this period some consolidation, such as formation of cell adhesion protein complexes (*closed ovals*), may be occurring at the target contact site.

Entry into the second or coupling phase was clearly demarcated by manifestations of force transduction between growth cones and target objects, resulting in filopodial stretching (Fig. 3 *a*) or neurite bending (Fig. 6 *a*). These forces appear to result from mechanical coupling of the targets to the underlying F-actin flow (Fig. 6) and are the same forces that drive retrograde translocation of beads (i.e., compliant objects) attached to lamellipodial or filopodial surfaces (Fig. 5). Interestingly, polycationic bead pseudotargets also exhibit a "contact phase" after binding to the growth cone surface: beads initially move randomly for a period of time that is inversely proportional to bead surface charge density before "coupling" to the retrograde F-actin flow (unpublished observations). These results suggest that functional growth cone–target coupling may involve gradual accumulation of a critical density of homophilic adhesion proteins capable of directly supporting or indirectly stimulating membrane-cytoskeletal linkage.

A successful coupling interaction was characterized by anterograde projection of the microtubule rich C domain along the target interaction axis (Fig 9 *b*, *coupling*). However, growth cone–target coupling alone clearly did not ensure directed microtubule extension; only coupling to a relatively noncompliant target did so. Bead pseudotargets, for example, become coupled to the actin flow but did not alter microtubule distribution or flow rate (Fig. 5). Similarly, semicompliant native targets such as the small caliber neurite in Fig. 6, were typically centripetally displaced by the flow toward the afferent growth cone's C domain but did not markedly affect microtubule distribution. In contrast, coupling to a larger noncompliant neurite, as illustrated in Fig. 4, resulted in rapid anterograde C domain extension. These results suggest that after the coupling event, growth cones attempt to "pull" on target substrates via attachment to actin filaments making up the retrograde flow. If the target is fully compliant (like a bead), passive retrograde displacement with the retrograde flow occurs and no growth cone–target tension develops; however, if the target is noncompliant, growth cone–target tension immediately develops. In the case of growth cone–growth cone interactions, a tug-of-war of F-actin appears to result with the "dominant cone" depleting actin networks from the "submissive cone" (cf., Fig. 3 *b*; note F-actin depletion from left cone proximal to interaction site and that the F-actin hot spot is displaced toward the dominant growth cone to the right). Interactions with noncompliant targets would be predicted to slow or even stop the retrograde flow. Consistent with this hypothesis, slowing of the retrograde F-actin flow specifically along the target interaction axis has been observed in preliminary experiments (Lin and Forscher, unpublished observations).

What could cause microtubule extension? As a membrane-cytoskeletal linkage forms between a noncompliant target and an afferent growth cone, the retrograde flow will tend to slow (Fig. 9 *b*, *smaller arrows* during *coupling* phase). If R_{flow} is decreased and R_- and R_+ remain relatively constant, a net anterograde flux of the P domain would result simply by actin network treadmilling, that is, continued leading edge assembly followed by eventual proximal network disassembly. Given microtubule elongation appears to be inhibited by the presence of distal actin filaments (Forscher and Smith, 1988), the resulting anterograde movement of the proximal F-actin boundary alone could promote microtubule elongation.

As an interaction matures, the growth cone enters a reorganization phase characterized by slow overall growth and intensive cytoskeletal remodeling, in particular microtubule reorientation along the target interaction axis. The final phase was characterized by accelerated outgrowth (Fig. 9 *b*). During this phase neurites often began a process of in vitro fasciculation as growth cones moved off the poly-L-lysine substrate and began migrating along target neurites (Fig. 4). Even partial transfer of the growth cone onto native neuronal growth substrates resulted in dramatic increases in outgrowth rates. Interestingly, despite roughly one order of magnitude increases in advance rates, the distribution of P and C cytoplasmic domains remained relatively constant (Fig. 4). This suggests that the ratio of R_+/R_- did not change significantly even after slowing of the actin flow. Acceleration might be explained by more efficient coupling (adhesion) between the F-actin and the native neuronal substrates; however, even the fastest measured rates of growth cone advance which approach 2 μm/min are somewhat slower than the typical R_{flow}. This implies that growth cones may never achieve the efficient coupling of actin assembly to forward advance (10 μm/min) reported in rapidly moving keratocytes (Theriot and Mitchison, 1991) perhaps due to tethering effects exerted by the axon. Cell specific differences may also come into play here: in addition to actin network assembly, growth cones probably need to generate forces to steer the axonal mass effectively during pathfinding decisions and thus may be endowed with molecular motors capable of producing relatively high levels of tension.

We have presented evidence that growth cone steering may result directly from perturbations of a steady state between polymer dynamics and mechanochemical processes underlying retrograde F-actin flow. A molecular substrate for the latter, presumably myosin-based process, still needs to be clarified despite the evidence for its existence. Our results show that microtubule guidance subsequent to growth cone–target recognition relies heavily on actin polymer dynamics and motility. Still missing from the growth cone guidance puzzle are molecular details of the target recognition response itself. Signaling mechanisms involved in coordinating the necessary membrane, cytoskeletal and mechanochemical processes are currently under investigation.

The authors gratefully acknowledge Corey Thompson for valuable suggestions and discussion throughout the course of this study. We also thank Dr.

William Bement, Dr. Richard Cheney and Dr. Joseph Wolenski, and other members of Dr. Mark Mooseker's lab for their insightful comments.

This work was supported by grants from the National Institutes of Health and the McKnight Endowment Fund for Neuroscience to P. Forscher and a fellowship from the Department of Education of Taiwan to C.-H. Lin.

Received for publication 22 January 1993 and in revised form 14 March 1993.

References

Abercrombie, M., J. E. M. Heaysman, and S. M. Pegrum. 1970. The locomotion of fibroblasts in culture. III. Movements of particles on the dorsal surface of the leading lamella. *Exp. Cell Res.* 62:389–398.

Bentley, D., and A. Toroian-Raymond. 1986. Disoriented pathfinding by pioneer neuron growth cone deprived of filopodia by cytochalasin treatment. *Nature (Lond.).* 323:712–715.

Bray, D. 1970. The surface movement during growth of single explanted neurons. *Proc. Natl. Acad. Sci. USA.* 65:905–910.

Bray, D. 1979. Mechanical tension produced by nerve cells in tissue culture. *J. Cell Sci.* 37:391–410.

Bray, D. 1984. Axonal growth in response to experimentally applied mechanical tension. *Dev. Biol.* 102:379–389.

Bridgman, P. C., and M. E. Dailey. 1989. The organization of myosin and actin in rapid frozen nerve growth cone. *J. Cell Biol.* 108:95–109.

Bridgman, P. C., B. Kachar, and T. S. Reese. 1986. The structure of cytoplasm in directly frozen cultured cells. II. Cytoplasmic domains associated with organelle movement. *J. Cell Biol.* 102:1510–1512.

Cheney, R. E., and S. M. Mooseker. 1992. Unconventional myosins. *Curr. Opin. Cell Biol.* 4:27–35.

Cooper, M. S., and M. Schliwa. 1985. Electrical and ionic controls of tissue cell locomotion in DC electrical fields. *J. Neurosci. Res.* 13:223–244.

Correas, I., R. Padilla, and J. Avila. 1990. The tubulin-binding sequence of brain microtubule-associated proteins, tau and MAP-2, is also involved in actin binding. *Biochem. J.* 269:61–64.

Danowski, B. A. 1989. Fibroblast contractility and actin organization are stimulated by microtubule inhibitors. *J. Cell Sci.* 93:255–266.

de Brabander, M., R. Nuydens, A. Ishihara, B. Holifield, K. Jacobson, and H. Geerts. 1991. Lateral diffusion and retrograde movements of individual cell surface components on single motile cells observed with Nanovid microscopy. *J. Cell Biol.* 112:111–124.

Dennerll, T. J., H. C. Joshi, V. L. Steel, R. E. Buxbaum, and S. R. Heidemann. 1988. Tension and compression in the cytoskeleton of PC12 neurites II: quantitative measurements. *J. Cell Biol.* 107:665–674.

Dennerll, T. J., P. Lamoureux, R. E. Buxbaum, and S. R. Heidemann. 1989. The cytomechanics of axonal elongation and retraction. *J. Cell Biol.* 109: 3073–3083.

Dodd, J., and T. M. Jessell. 1988. Axon guidance and the patterning of neuronal projections in vertebrates. *Science (Wash. DC).* 242:692–699.

Euteneuer, U., and M. Schliwa. 1985. Evidence for an involvement of actin in the positioning and motility of centrosomes. *J. Cell Biol.* 101:96–103.

Euteneuer, U., and M. Schliwa. 1992. Mechanism of centrosome positioning during the wound response in BSC-1 cells. *J. Cell Biol.* 116:1157–1166.

Forscher, P., and S. J. Smith. 1988. Actions of cytochalasins on the organization of actin filaments and microtubules in a neuronal growth cone. *J. Cell Biol.* 107:1505–1516.

Forscher, P., and S. J. Smith. 1990. Cytoplasmic actin filaments move particles on the surface of a neuronal growth cone. Optical Microscopy for Biology. Wiley Liss, Inc., New York. 1990. 459–471.

Forscher, P., C. H. Lin, and C. Thompson. 1992. Novel form of growth cone motility involving site-directed actin filament assembly. *Nature (Lond.).* 357:515–518.

Forscher, P., L. K. Kaczmarek, J. Buchanan, and S. J. Smith. 1987. Cyclic AMP induced changes in distribution and transport of organelles within growth cones of *Aplysia* bag cell neurons. *J. Neurosci.* 7:3600–3611.

Goodman, C. S., M. J. Bastiani, C. Q. Doe, S. du Lac, S. L. Helfand, J. Y. Kuwada, and J. B. Thomas. 1984. Cell recognition during neuronal cell development. *Science (Wash. DC).* 225:1271–1279.

Goslin, K., E. Birgbauer, G. Banker, and F. Solomon. 1989. The role of cytoskeleton in organizing growth cones: a microfilament-associated growth cone component depends upon microtubules for its localization. *J. Cell Biol.* 109:1621–1631.

Griffith, L. M., and T. D. Pollard. 1978. Evidence for actin filament-microtubule interaction mediated by microtubule-associated proteins. *J. Cell Biol.* 958–965.

Gundersen, R. W., and J. N. Barrett. 1980. Characterization of the turning response of dorsal root neurites toward nerve growth factor. *J. Cell Biol.* 87:546–554.

Harrison, R. G. 1910. The outgrowth of the nerve fiber as a mode of protoplasmic movement. *J. Exp. Zool.* 17:521–544.

Heidemann, S. R., P. Lamoureux, and R. E. Buxbaum. 1990. Growth cone behavior and production of traction force. *J. Cell Biol.* 111:1949–1957.

Hortsch, M., and C. S. Goodman. 1991. Cell and substrate adhesion molecules in Drosophila. *Annu. Rev. Cell Biol.* 7:505–557.

Jessell, T. M. 1988. Adhesion molecules and the hierarchy of neural development. *Neuron.* 1:3–13.

Kaczmarek, L. K., M. Finbow, J. P. Revel, and F. Strumwasser. 1979. The morphology and coupling of *Aplysia* bag cells within the abdominal ganglion and in cell culture. *J. Neurobiol.* 10:525–550.

Kucik, D. F., E. L. Elson, and M. P. Sheetz. 1989. Forward transport of glycoproteins on leading lamellipodia in locomoting cells. *Nature (Lond.).* 340: 315–317.

Kuznetsov, S. A., G. M. Langford, and D. G. Weiss. 1992. Actin-dependent organelle movement in squid axoplasm. *Nature (Lond.).* 356:722–725.

Lamoureux, P., R. E. Buxbaum, and S. R. Heidemann. 1989. Direct evidence that growth cones pull. *Nature (Lond.).* 340:159–162.

Lamoureux, P., J. Zheng, R. E. Buxbaum, and S. R. Heidemann. 1992. A cytomechanical investigation of neurite growth on different culture surfaces. *J. Cell Biol.* 118:655–661.

Lasek, R. 1986. Polymer sliding in axons. *J. Cell Sci. 5 (suppl.):*161–179.

Letourneau, P. C., and T. A. Shattuck. 1989. Distribution and possible interactions of actin-associated proteins and cell adhesion molecules of nerve growth cones. *Development* 105:505–519.

Letourneau, P. C., T. A. Shattuck, and A. H. Ressler. 1987. "Pull" and "push" in neurite elongation: observations on the effects of different concentrations of cytochalasin-B and taxol. *Cell Motil. Cytoskeleton.* 8:193–209.

Lewis, A. K., and P. C. Bridgman. 1992. Nerve growth cone lamellipodia contain two populations of actin filaments that differ in organization and polarity. *J. Cell Biol.* 119:1219–1243.

Marsh, L., and P. C. Letourneau. 1984. Growth of neurites without filopodial or lamellipodial activity in the presence of cytochalasin B. *J. Cell Biol.* 99:2041–2047.

Miller, M., E. Bower, P. Levitt, D. Li, and P. D. Chantler. 1992. Myosin II distribution in neurons is consistent with a role in growth cone motility but not synaptic vesicle mobilization. *Neuron.* 8:25–44.

Mitchison, T., and M. Kirschner. 1988. Cytoskeletal dynamics and nerve growth. *Neuron.* 1:761–772.

Morales, M., and E. Fifkova. 1989. Distribution of MAP2 in dendritic spines and its colocalization with actin: an immuno-gold electron-microscope study. *Cell Tissue Res.* 256:447–456.

O'Connor, T. P., J. S. Duerr, and D. Bentley. 1990. Pioneer growth cone steering decisions mediated by single filopodial contacts in situ. *J. Neurosci.* 10:3935–3946.

Okabe, S., and N. Hirokawa. 1991. Actin dynamics in growth cones. *J. Neurosci.* 11:1918–1929.

Patel, N., and M.-M. Poo. 1982. Orientation of neurite growth by extracellular electric fields. *J. Neurosci.* 2:483–496.

Peng, H. B., and P. C. Cheng. 1982. Formation of postsynaptic specialization induced by latex beads in cultured muscle cells. *J. Neurosci.* 2:1760–1774.

Peng, H. B., D. R. Markey, W. L. Muhlach, and E. M. Pollack. 1987. Development of presynaptic specializations induced by basic polypeptide-coated latex beads in spinal cord cultures. *Synapse (NY).* 1:10–19.

Ramon y Cajal, S. 1890. Sur l'origine et les ramifications des fibres nerveuses de la moelle embryonaire. *Anat. Anz.* 5:609–613.

Reichardt, L. F., and K. J. Tomaselli. 1991. Extracellular matrix molecules and their receptors: functions in neural development. *Annu. Rev. Neurosci.* 14:531–570.

Sabry, J. H., T. P. O'Connor, L. Evans, R. A. Toroian, M. Kirschner, and D. Bentley. 1991. Microtubule behavior during guidance of pioneer neuron growth cones in situ. *J. Cell Biol.* 115:381–395.

Schliwa, M., and J. Van Blerkom. 1981. Structural interaction of cytoskeletal components. *J. Cell Biol.* 90:222–235.

Selden, S. C., and T. D. Pollard. 1983. Phosphorylation of microtubule-associated proteins regulates their interactions with actin filaments. *J. Biol. Chem.* 258:7064–7071.

Sheetz, M. P., S. Turney, H. Qian, and E. L. Elson. 1989. Nanometre-level analysis demonstrates that lipid flow does not drive membrane glycoprotein movements. *Nature (Lond.).* 340:284–288.

Shpetner, H., and R. Vallee. 1989. Identification of dynamin, a novel mechanochemical enzyme that mediates interactions between microtubules. *Cell.* 59:421–432.

Smith, S. J. 1988. Neuronal cytomechanics: the actin-based motility of growth cones. *Science (Wash. DC).* 242:708–715.

Takeichi, M. 1991. Cadherin cell adhesion receptors as a morphogenetic regulator. *Science (Wash. DC).* 251:1451–1455.

Tanaka, E. M., and M. W. Kirschner. 1991. Microtubule behavior in the growth cones of living neurons during axon elongation. *J. Cell Biol.* 115:345–363.

Tessier, L. M., M. Placzek, A. G. Lumsden, J. Dodd, and T. M. Jessell. 1988. Chemotropic guidance of developing axons in the mammalian central nervous system. *Nature (Lond.).* 336:775–778.

Theriot, J. A., and T. J. Mitchison. 1991. Actin microfilament dynamics in locomoting cells. *Nature (Lond.).* 352:126–131.

Theriot, J. A., and T. J. Mitchison. 1992. Comparison of actin and cell surface dynamics in motile fibroblasts. *J. Cell Biol.* 119:367–377.

Travis, J. L., and S. S. Bowser. 1986. Microtubule-dependent reticulopodial motility: is there a role for actin? *Cell Motil. Cytoskeleton.* 6:146–152.